Defense Threat Reduction Agency
8725 John J. Kingman Road, MS
6201 Fort Belvoir, VA 22060-6201

DTRA-TR-13-43

TECHNICAL REPORT

High-Resolution Structural Monitoring of Ionospheric Absorption Events

Approved for public release; distribution is unlimited.

July 2013

HDTRA1-03-D-0009

Lee J. Rickard

Prepared by:
OVPR/University Strategic Partnership
MSC02 1660
1 University of New Mexico
Albuquerque, NM 87131

DESTRUCTION NOTICE:

Destroy this report when it is no longer needed.
Do not return to sender.

PLEASE NOTIFY THE DEFENSE THREAT REDUCTION AGENCY, ATTN: DTRIAC/ J9CXTP, 8725 JOHN J. KINGMAN ROAD, MS-6201, FT BELVOIR, VA 22060-6201, IF YOUR ADDRESS IS INCORRECT, IF YOU WISH THAT IT BE DELETED FROM THE DISTRIBUTION LIST, OR IF THE ADDRESSEE IS NO LONGER EMPLOYED BY YOUR ORGANIZATION.

REPORT DOCUMENTATION PAGE

Form Approved
OMB No. 0704-0188

1. REPORT DATE *(DD-MM-YYYY)*	2. REPORT TYPE	3. DATES COVERED *(From - To)*
00-07-2013	Technical	07/21/2010 - 4/30/2012

4. TITLE AND SUBTITLE
High-Resolution Structural Monitoring of Ionospheric Absorption Events

5a. CONTRACT NUMBER

5b. GRANT NUMBER
DTRA01-03-D-0009-0026

5c. PROGRAM ELEMENT NUMBER

6. AUTHOR(S)
Lee J. Rickard

5d. PROJECT NUMBER
8

5e. TASK NUMBER
26

5f. WORK UNIT NUMBER

7. PERFORMING ORGANIZATION NAME(S) AND ADDRESS(ES) AND ADDRESS(ES)
OVPR / University Strategic Partnership
MSC02 1660
1 University of New Mexico
Albuquerque,New Mexico 87131

8. PERFORMING ORGANIZATION REPORT NUMBER
798B

9. SPONSORING / MONITORING AGENCY NAME(S) AND ADDRESS(ES)
Defense Threat Reduction Agency
8725 John J. Kingman Rd. STOP 6201
6201 Fort Belvoir, VA 22060
PM/J. Reed

10. SPONSOR/MONITOR'S ACRONYM(S)
DTRA

11. SPONSOR/MONITOR'S REPORT NUMBER(S)
DTRA-TR-13-43

12. DISTRIBUTION / AVAILABILITY STATEMENT
Approved for public release; distribution is unlimited.

13. SUPPLEMENTARY NOTES

14. ABSTRACT

Under this task, we have augmented the hardware of the Long Wavelength Array (LWA) to provide a significant riometric capability, in order to search for anomalous absorption events that are associated with radiation belt precipitation events. Although limitations arising from initial data quality and radio frequency interference (RFI) have slowed implementation, the DTRA-supported augmentations are being incorporated into the standard data flow of the Prototype All-Sky Imager (PASI), in order to give real-time, 24/7 riometry. Incorporation of an outrigger site, to enable treatment of the unknown structure of the celestial background and the effects of confusion noise, was completed. However, RFI issues have prevented combination of outrigger data with LWA1.

15. SUBJECT TERMS
radiation belts, particle precipitation events, radio interferometry, ionosphere

16. SECURITY CLASSIFICATION OF:			17. LIMITATION OF ABSTRACT	18. NUMBER OF PAGES	19a. NAME OF RESPONSIBLE PERSON
a. REPORT	b. ABSTRACT	c. THIS PAGE			Dr. Lee J Rickard
U	U	U	UU	21	19b. TELEPHONE NUMBER *(include area code)* (703) 589-3675

CONVERSION TABLE

Conversion Factors for U.S. Customary to metric (SI) units of measurement.

MULTIPLY →	BY →	TO GET
TO GET ←	BY ←	DIVIDE
angstrom	1.000 000 x E -10	meters (m)
atmosphere (normal)	1.013 25 x E +2	kilo pascal (kPa)
bar	1.000 000 x E +2	kilo pascal (kPa)
barn	1.000 000 x E -28	meter^2 (m^2)
British thermal unit (thermochemical)	1.054 350 x E +3	joule (J)
calorie (thermochemical)	4.184 000	joule (J)
cal (thermochemical/cm^2)	4.184 000 x E -2	mega joule/m^2 (MJ/m^2)
curie	3.700 000 x E +1	*giga bacquerel (GBq)
degree (angle)	1.745 329 x E -2	radian (rad)
degree Fahrenheit	t_k = (t°f + 459.67)/1.8	degree kelvin (K)
electron volt	1.602 19 x E -19	joule (J)
erg	1.000 000 x E -7	joule (J)
erg/second	1.000 000 x E -7	watt (W)
foot	3.048 000 x E -1	meter (m)
foot-pound-force	1.355 818	joule (J)
gallon (U.S. liquid)	3.785 412 x E -3	meter^3 (m^3)
inch	2.540 000 x E -2	meter (m)
jerk	1.000 000 x E +9	joule (J)
joule/kilogram (J/kg) radiation dose absorbed	1.000 000	Gray (Gy)
kilotons	4.183	terajoules
kip (1000 lbf)	4.448 222 x E +3	newton (N)
kip/inch^2 (ksi)	6.894 757 x E +3	kilo pascal (kPa)
ktap	1.000 000 x E +2	newton-second/m^2 (N-s/m^2)
micron	1.000 000 x E -6	meter (m)
mil	2.540 000 x E -5	meter (m)
mile (international)	1.609 344 x E +3	meter (m)
ounce	2.834 952 x E -2	kilogram (kg)
pound-force (lbs avoirdupois)	4.448 222	newton (N)
pound-force inch	1.129 848 x E -1	newton-meter (N-m)
pound-force/inch	1.751 268 x E +2	newton/meter (N/m)
pound-force/foot^2	4.788 026 x E -2	kilo pascal (kPa)
pound-force/inch^2 (psi)	6.894 757	kilo pascal (kPa)
pound-mass (lbm avoirdupois)	4.535 924 x E -1	kilogram (kg)
pound-mass-foot^2 (moment of inertia)	4.214 011 x E -2	kilogram-meter^2 (kg-m^2)
pound-mass/foot^3	1.601 846 x E +1	kilogram-meter^3 (kg/m^3)
rad (radiation dose absorbed)	1.000 000 x E -2	**Gray (Gy)
roentgen	2.579 760 x E -4	coulomb/kilogram (C/kg)
shake	1.000 000 x E -8	second (s)
slug	1.459 390 x E +1	kilogram (kg)
torr (mm Hg, 0^0 C)	1.333 22 x E -1	kilo pascal (kPa)

*The bacquerel (Bq) is the SI unit of radioactivity; 1 Bq = 1 event/s.

**The Gray (GY) is the SI unit of absorbed radiation.

HIGH-RESOLUTION STRUCTURAL MONITORING OF IONOSPHERIC ABSORPTION EVENTS

FINAL REPORT
UNM_DTRA01-03-D-0009-0026_Project 8

SUMMARY

Under this task, the hardware of the Long Wavelength Array (LWA) has been augmented to provide a significant riometric capability, in order to search for anomalous absorption events that are associated with radiation belt precipitation events. Although limitations arising from initial data quality and radio frequency interference (RFI) have slowed implementation, the DTRA-supported augmentations are being incorporated into the standard data flow of the Prototype All-Sky Imager (PASI), in order to give real-time, 24/7 riometry. Incorporation of an outrigger site, to enable treatment of the unknown structure of the celestial background and the effects of confusion noise, was completed. However, RFI issues have prevented combination of outrigger data with LWA1.

This 6.2 work is in support of the Basic and Applied Sciences Directorate and the JSTO and the DTRA FY 2009 call for Basic Research in Countering-WMD, under the specific topic area of The Physics of Artificial Radiation Belt Formation and Decay (Topic H).

I. BACKGROUND

A crucial element of the DTRA mission is to understand the dynamics of the Van Allen radiation belts, because artificial enhancements of the radiation belts could have catastrophic impacts on space systems, as well as on terrestrial systems that are influenced by the ionospheric response to changes in the radiation belts. A measure of these dynamics is the precipitation of beta particles from the radiation belts to lower altitudes; these precipitation events are driven by the dynamics of wave-particle interactions in the radiation belts. One specific problem, then, is to understand the dynamics provoking these events by matching them to potential stimuli (solar events, lightning, etc.).

Interest in these phenomena originated because Department of Defense models of artificial radiation belts produced by high altitude nuclear detonations had large uncertainties in peak intensity and duration, in part because of poorly understood mechanisms for beta depletion. Recent experimental evidence shows that wave-particle interactions are significant factors in both beta acceleration and beta loss in the natural radiation belts[1]. Among the natural processes that are now known to induce electron precipitation are lightning, through generation of whistler-mode waves[2], earthquakes, through generation of ultra-low frequency (ULF) and very-low frequency (VLF) waves[3], and, the direct distortion of the magnetosphere by solar flares and coronal mass ejections (CMEs)[4].

The precipitating electrons cause localized ionization and changes of ionospheric plasma conductivity[5]. This results in enhanced absorption of the cosmic high frequency (HF; typically 10 – 60 MHz) radio background, originating primarily in the D-region, the lowest part of the ionosphere. Such enhanced, or anomalous, absorption measurements have been the subject of ground-based studies since before the original International Geophysical Year[6]. The method

currently used for such studies is riometry, and has remained relatively unchanged for almost as long[7].

In riometry, a long time-series of observations is used to determine a 'quiet background level', which is a convolution of the system response and the (strong) Galactic background, and varies slowly on an hourly and yearly basis. Anomalous absorption measurements are detected as shorter term variations in which the observed flux drops, perhaps by tens of dB. An example is shown in figure 1, taken from observations by the 30 MHz riometer operating at the High Frequency Active Auroral Research Program (HAARP) facility in Alaska. The quiet background level, determined over many days, is the green line; the riometer signal (blue line) tracks it well until 1400 hours on the 29th. The sharp dips in the detector signal are the absorption events. They have been converted to absorption (in dB) and shown as the red line. Note the significant depths of the absorption events, approaching 3 dB (a reduction in half of the signal strength).

Correlation of these events with electron precipitation can be shown directly in the case of the 20 November 2003 geomagnetic storm, for which a riometric event occurs at the time that L-shell electron depletion is measured by satellite (figures 2 and 3). Figure 2 shows the omnidirectional integrated energetic electron fluxes for several energy thresholds, as measured[8] by the Highly Elliptical Orbiter HEO-3. The 20 November event is very prominent, beginning at roughly 1200 UTC and persisting for the next two days. Figure 3 shows two records from the HAARP 30 MHz riometer, pasted together to cover 20 November 2003. While the ionosphere is disturbed both before and after the event, the time of the onset of the major precipitation event corresponds very well to the large, coherent absorption event, starting at 1200 UTC and persisting through the length of the available record.

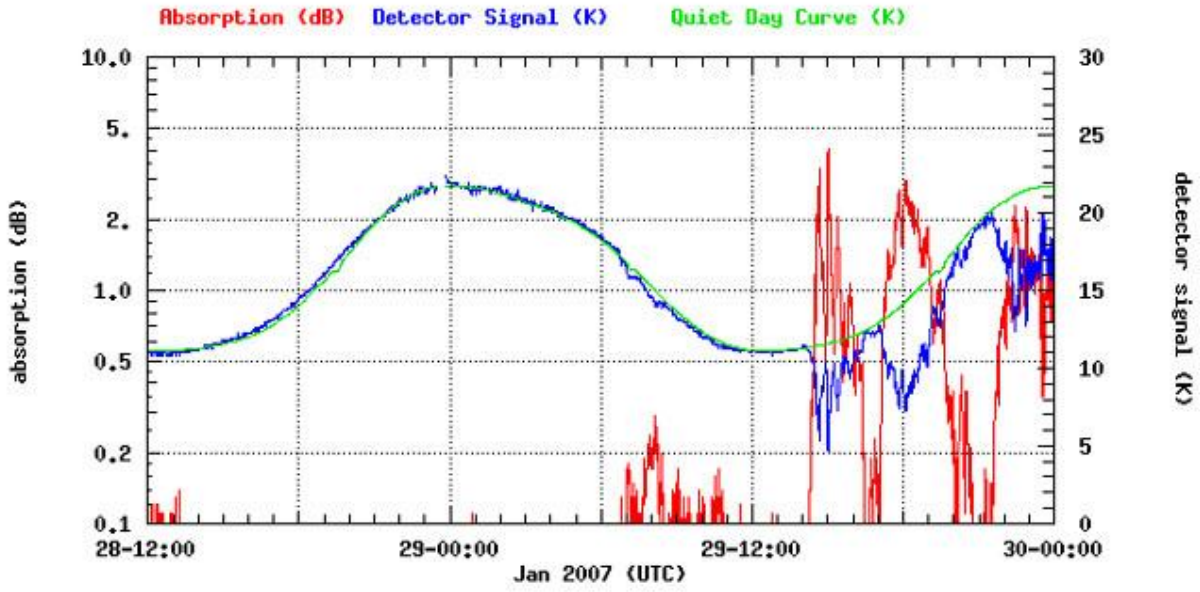

Figure 1: Anomalous absorption event seen by HAARP 30 MHz riometer.

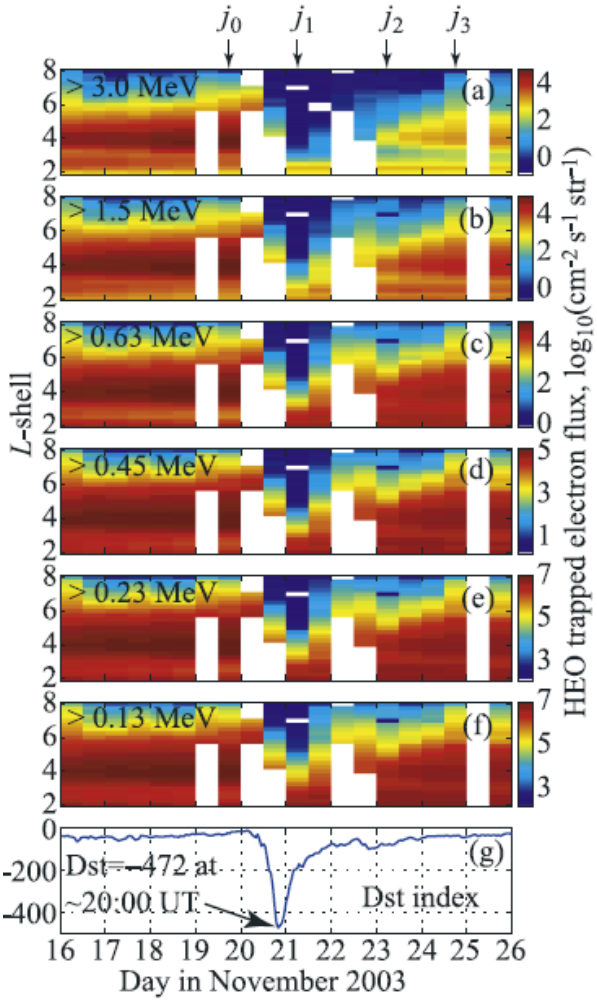

Figure 2: Electron depletion event[8] observed by HEO-3 satellite on 20 November 2003.

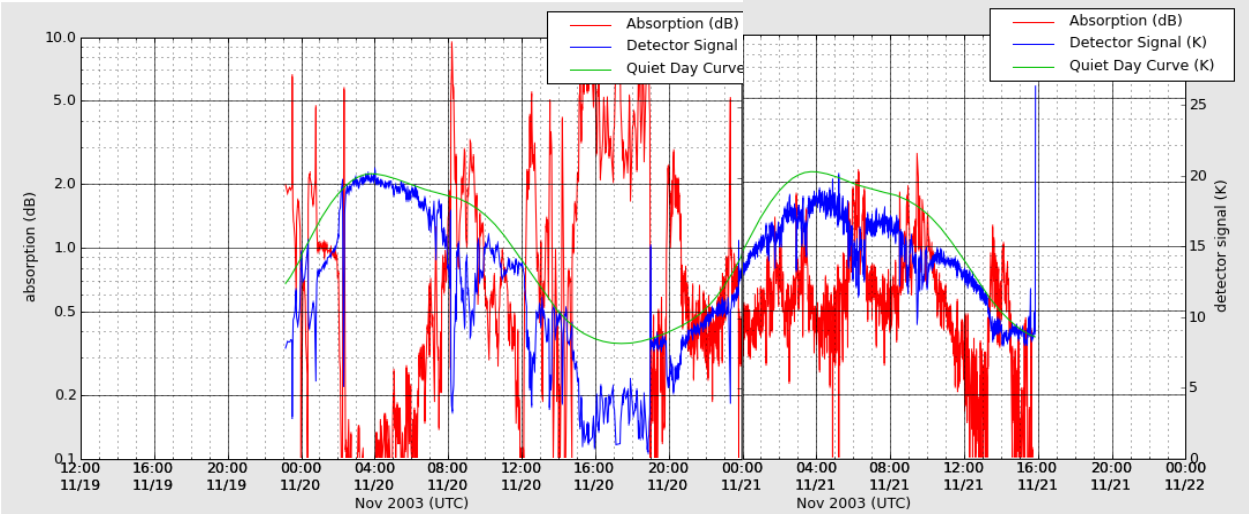

Figure 3: Correlated riometer event appears in HAARP 30 MHz data.

Additional information can be gleaned from the spatial distribution of the absorption event. To date, this has been done by using small arrays of antennas (typically 4x4 or 8x8) and analog beam formation (via Butler matrices), to generate a set of beams on the sky. The spatial resolution is coarse: figure 4a shows the beams generated with the IRIS system at Kilpisjarvi, Finland, which operates at 38.2 MHz; the distance scale is derived by projecting the beams to the altitude of the D-region. Figure 4b shows an anomalous absorption event captured with this system. Note that, even at this fairly coarse resolution, there is discrete structure that changes in position and strength over time. That indicates that observations with higher angular resolution could reveal even more information about the events.

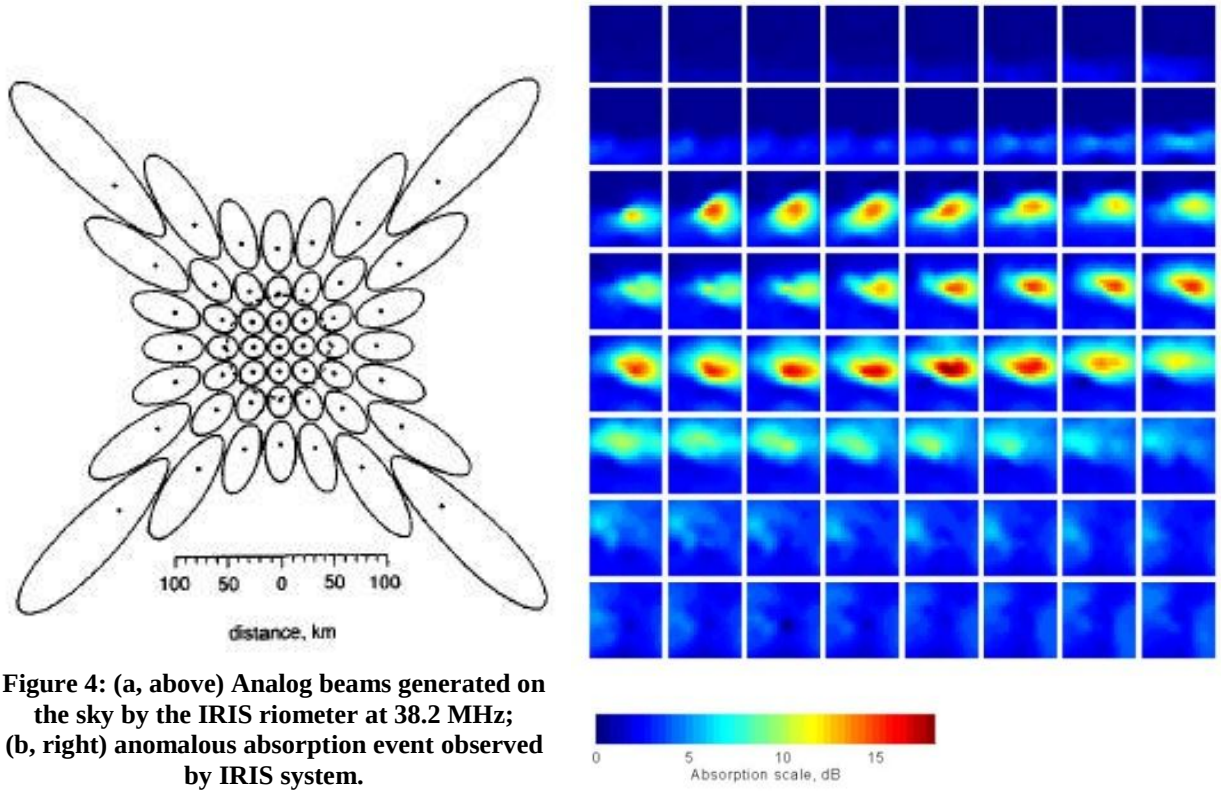

Figure 4: (a, above) Analog beams generated on the sky by the IRIS riometer at 38.2 MHz; (b, right) anomalous absorption event observed by IRIS system.

One of the principal limitations of single antenna or small array riometry is the difficulty of determining the quiet background. The reason for this can be seen in figure 5, which has been taken from the documentation for the CANOPUS riometer array, originally developed by the University of Calgary and now part of the Canadian Norstar program[9]. The figure shows the Galactic background at 22 MHz, provided by Tom Landecker of the Dominion Radio Astronomy Observatory. The small circle is the instantaneous field-of-view of the CANOPUS riometer at Pinawa; this field-of-view is swept around the North Celestial Pole over the course of a day. It is clear that the structure of the background, dominated by the complexity of the Galactic emission, varies in the riometer data. This requires an elaborate process for determining an empirical quiet day curve.

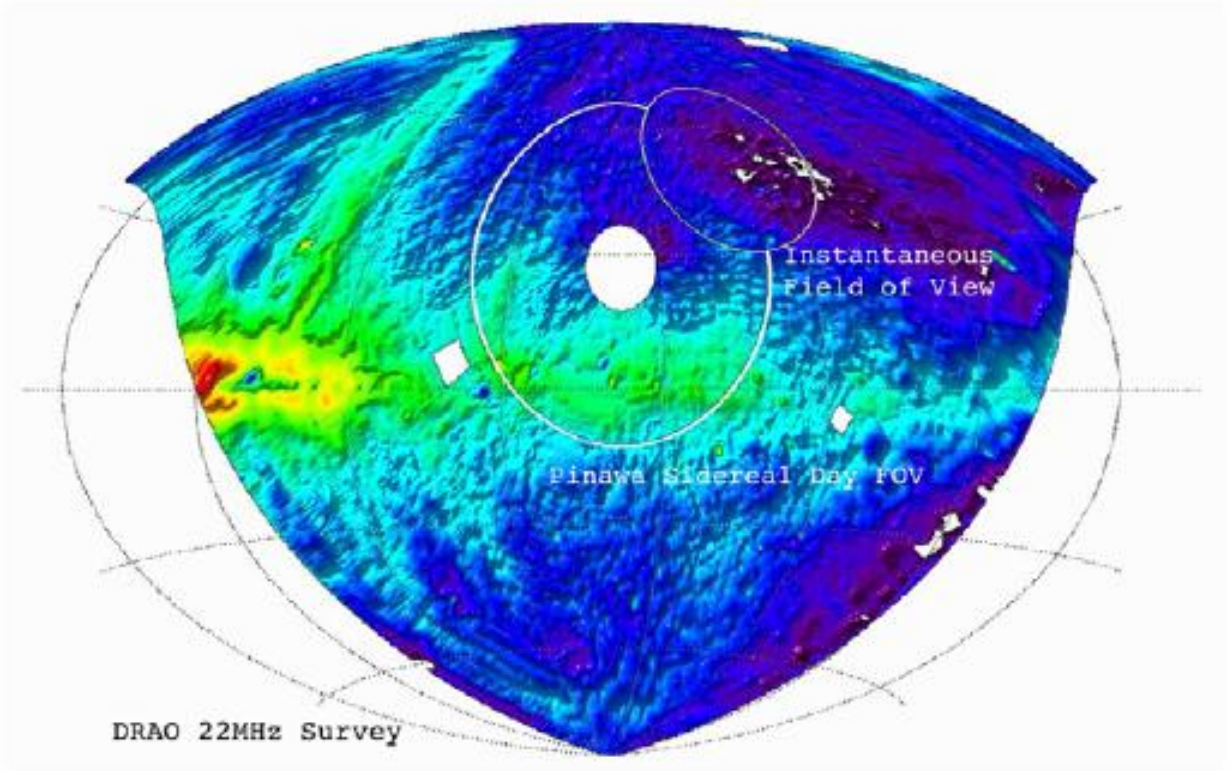

Figure 5: Superimposed on the 22 MHz DRAO image of the background Galactic emission are (small circle) the instantaneous field of view of the Pinawa riometer, and (large circle) the path it sweeps out over the course of a sidereal day. The blank circle within the sidereal path is the region of the North Celestial Pole, which cannot be observed by the DRAO instrument.

Yet, if the angular resolution were improved, and if the sky against which the riometric measurement is made could be *imaged*, then the sky itself would provide a simpler calibration scheme. At low frequencies, the sky has numerous background radio sources that are effectively point sources as seen by the riometer; these sources have been measured by astronomical instruments over a range of frequencies, enabling the prediction of their absolute brightnesses at the riometer frequency, and thus a calibration of the flux scale that can be transferred to the Galactic background. Imaging would then enable isolation of the absorption measurements against the calibrated background, and would provide a plethora of measurements in each image.

II. INSTRUMENTAL WORK

The objective proposed for this work was to develop an instrumental capability to address the problems discussed above by simultaneously imaging the sky background and resolving the fine-scale structure of ionospheric absorption events. Rather than starting from zero, the work was built on top of an existing instrument, not funded by DTRA – a new low-frequency radio array for advanced astrophysics and space physics experiments. It had been hoped that this instrument could provide a significant new riometric capability, but that was not part of the original project baseline. The intent for this work was to develop the required software for analyzing all-sky data, and to augment the performance of the instrument by adding an 'outlier', to address both the angular resolution and the confusion noise (discussed below) of the baseline facility. Once those elements were complete, it was anticipated that detection of anomalous

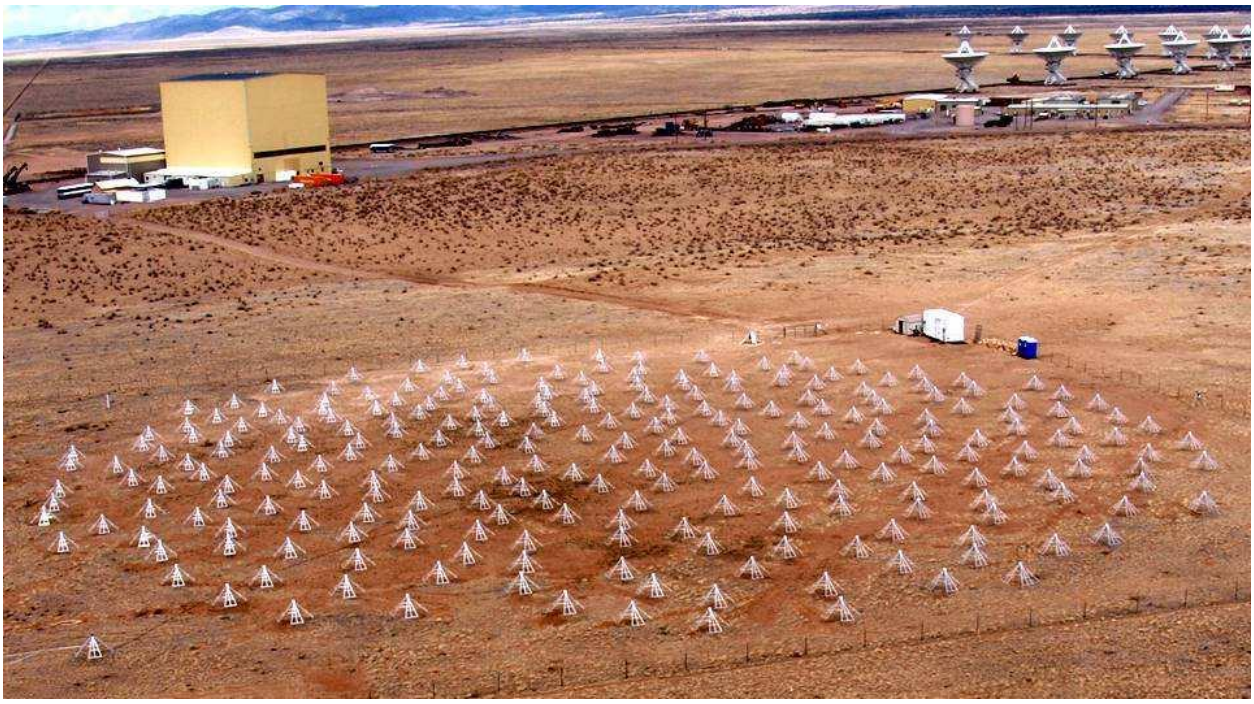

Figure 6: Aerial view of LWA1, the first station of the Long Wavelength Array. The radio dishes to the upper right are part of the Jansky Very Large Array, in compact configuration.

absorption events and correlation of their occurrence and evolution with data for potential triggering mechanisms would improve our understanding of the driving physics for radiation belt precipitation events.

LWA1 is the first station of the Long Wavelength Array (LWA), located near the center of the Jansky Very Large Array (JVLA) on the Plains of San Agustin, New Mexico. Extensive details on the technical decisions behind LWA1 have been, published[10] and a full report on the completed station has been submitted for publication[11]. Thus, only a summary will be given here.

LWA1 consists of 256 antenna stands, each comprising two broadband, crossed, linearly-polarized dipoles, laid out over a roughly 100-meter diameter station. The distribution of stands is pseudorandom, to prevent aliasing of the main lobe and to reduce the size of the sidelobes at higher frequencies where the aperture will be undersampled. After amplification at the front end and transmission over coaxial cable to the electronics shelter (at the upper right corner of the array in figure 6), each polarization is filtered and amplified by an analog receiver. The resulting signal is sky-noise dominated (>4:1) over the region from 24 to 87 MHz, which is critical for riometric applications.

The signals are then direct-sampled at 196 Msps by the A/D converter. A time-domain delay-and-sum architecture allows the entire 10–88 MHz passband from each antenna to be processed as a single wideband data stream. Delays are implemented in two stages: A coarse delay is implemented using a first-in first-out (FIFO) buffer operating on the A/D output samples, followed by a finite impulse response (FIR) filter for sub-sample delay. The signals are then added to the signals from other antennas processed similarly. Four simultaneous, dual-polarization beams of bandwidth 78 MHz, each capable of fully independent pointing over the visible sky, can be constructed in this fashion. Each beam can be steered to any point on the sky

on millisecond timescales by adjusting the digital delays of the individual elements; this beam steering is done entirely electronically, controlled by the station software.

Each full-bandwidth beam is down-converted by a digital receiver and sent to a polyphase filter bank to channelize the beams into spectral channels. With 4096 channels, beam bandwidths up to 16 MHz and spectral resolutions down to 61 Hz are achieved. Two "tunings" can be extracted from any frequency in the 78 MHz-wide passband for each beam. The station beam can be steered to any point in the sky on millisecond timescales by adjusting the digital delays of the individual elements. Beam steering is entirely electronic.

In addition, and of primary importance to this project, the station electronics can coherently capture and record the output of all A/Ds, where each A/D corresponds to one antenna. There are two modes: the "transient buffer – wideband" (TBW) allows the raw output of the A/Ds to be collected continuously for 57 ms at a time. The "transient buffer – narrowband" (TBN) allows a single tuning of 75 kHz bandwidth to be streamed continuously. These buffers enable the production of truly all-sky imagery, while the normal beams can only produce near-simultaneous wide-field imagery through rapid electronic beam steering.

An example 23 MHz TBN image is shown in figure 7. The primary feature is the Galactic plane, crossing the middle of the image. Jupiter, whose emission at 23 MHz is dominated by the decametric (burst) radiation linked to Io, is the bright source on the left side. The other bright sources ranged around the horizon are radio-frequency interference (RFI) emissions. As a point source, Jupiter shows the station beam size; the full-width at half-maximum (FWHM) is expected to be [8°, 2°] at [20, 80] MHz at the zenith.

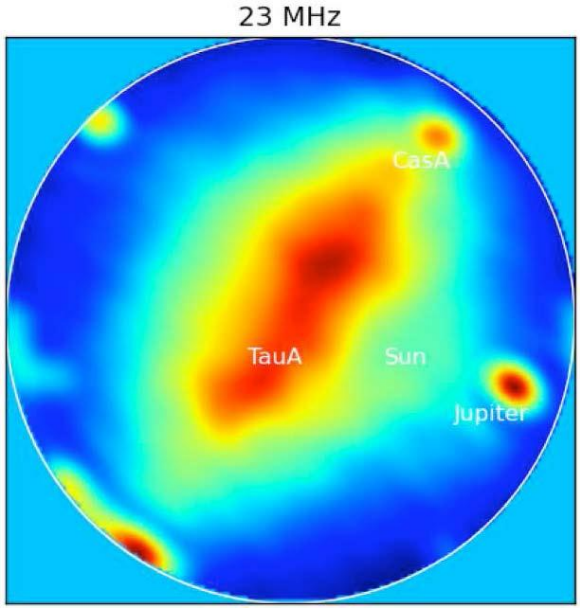

Figure 7: All-sky LWA1 TBN 23 MHz image showing Galactic-background limited operation.

With additional support from Los Alamos National Laboratory, an additional all-sky imaging element has been incorporated. The Prototype All-Sky Imager (PASI) is a software-defined correlator/imager that runs off the TBN data stream. Using a cluster of four server-class computers with Nahalem multicore processors interconnected by an Infiniband switch, PASI cross-correlates the dipole data streams, producing a sampling of visibilities within the station aperture. These visibilities are then transformed into sky images as in any interferometric imager. PASI uses the NRAO Common Astronomy Software Applications (CASA) software library for its post-processing.

PASI images nearly the whole sky 12 times per minute, continuously and in real time, with a duty cycle of 95% or better. In fact, the PASI images are posted in real-time on the LWA web site (at http://www.phys.unm.edu/~lwa/lwatv.html). Images for the Stokes I (intensity) and Stokes V (circularly polarized emission) are displayed for whatever frequency LWA1 happens to be operating at. Because of the all-sky, real-time aspect of the PASI data, it was felt that this would be the best data stream on which to establish the riometric procedure.

Several things should be noted: (1) there are excellent models for the diffuse galactic emission at low frequencies, so one can derive opacity directly against it; (2) aside from Jupiter, there are strong point sources, such as Cas A and Tau A, which also have excellent emission models, so that one can derive overall gain calibrations from them; (3) one can move over a large frequency range to distinguish spectral behavior of background and foreground; and (4) one can use unpolarized celestial sources to verify polarization calibration.

Initial observations with LWA1 were made in the Spring of 2011. Unfortunately, the TBN data showed a severe RFI problem, whose intensity was so great that it was not possible to reach the celestial background (figure 8). This prompted an extensive search over the vicinity of the station for the responsible emitter, which was lengthened by the need for multiple interactions both with NRAO and with the local power company, the Socorro Electric Cooperative. In July, the problem was finally identified as coming from a switch on a nearby power pole (figure 9) that had deteriorated enough to be an RFI problem, but not so much as to attract the attention of the power company's maintenance crews. In addition to delaying work on the TBN data, this was a warning of things to come (discussed below).

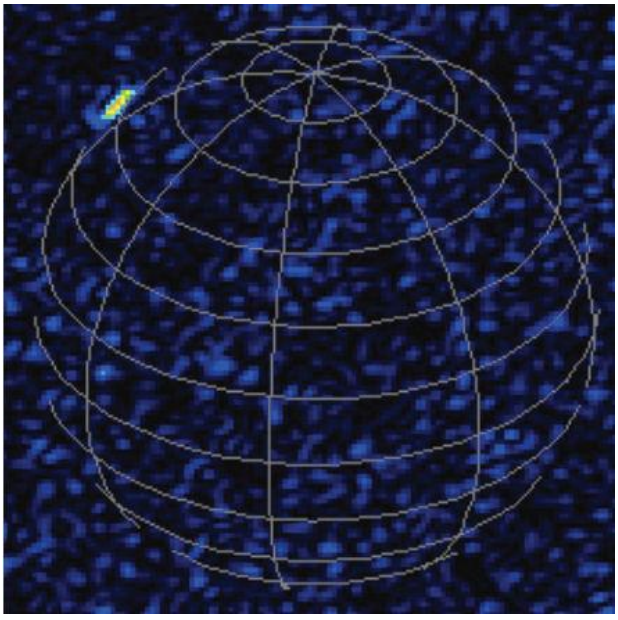

Figure 8: All-sky LWA1 TBN image overwhelmed by RFI source (upper left).

Figure 9: Identification of the source of the RFI in figure 8.

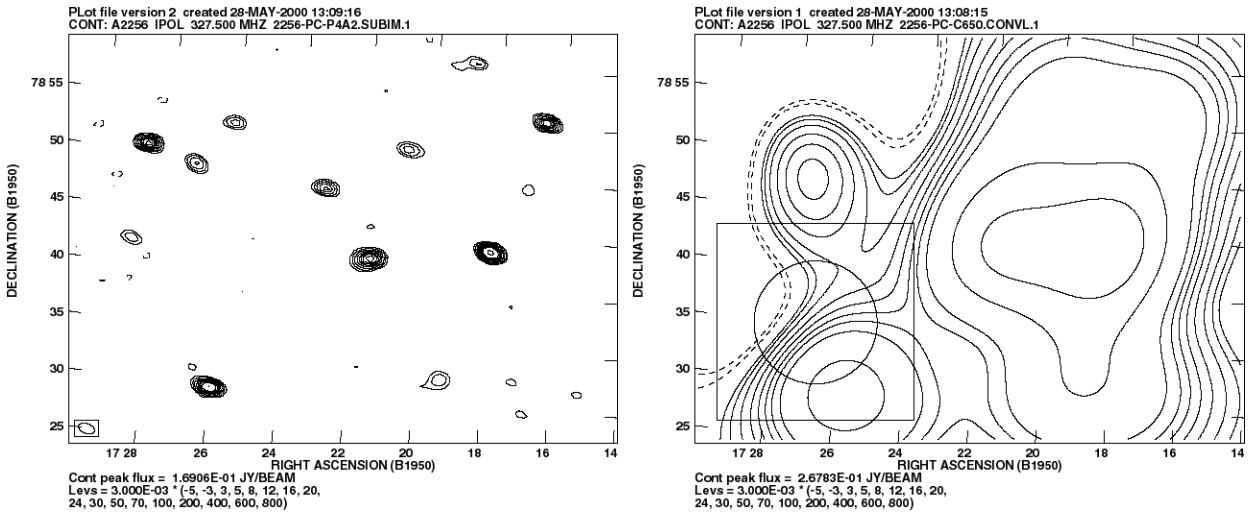

Figure 10: (a) Background point sources observed with an angular resolution of one arc-minute. (b) Same field of point sources convolved to an angular resolution of ten arc-minutes.

The large station beam size suggests another complication that must be addressed: source confusion. Figure 10 demonstrates this issue. Figure 10a shows a random field of background point sources, observed with a beam FWHM of one arc-minute. The RMS noise in this image is 3 mJy/beam. Figure 10b shows the same map, convolved to a beam FWHM of ten arc-minutes. It is obvious that the larger beam (the circle in the lower left) sees a lot of apparent background fluctuation that arises from the merging of sources. The result is an image RMS noise of 30 mJy/beam. This increased noise is the confusion noise.

Because of this effect, it was felt that it would be important to improve the angular resolution of the LWA1 station, by incorporating baselines (antenna separations) much larger than the 100m scale of the station. LWA1 is intended to be the first of 53 stations in the final Long Wavelength Array; leases have already been obtained for several new station sites. It was decided to develop the LWA1 'outrigger' at the site intended for LWA2, which is roughly 1 km from the end of the north arm of the JVLA, and roughly 20 km from LWA1.

The initial plan was to link the outrigger to LWA1 by installing a data fiber link to the JVLA. However, the time-scale for doing this turned out to be incompatible with the desired timeline for the DTRA contract. The back-up plan was to install data recorders similar to those used in LWA1 and physically carry the data back to another site for correlation after the fact.

Installation of the outrigger station began in the summer of 2011. Twenty antenna stands were laid out over an extent of 100m, at postiions selected from the pseudorandom distribution used for LWA1. The analog electronics from LWA1 were duplicated for the outrigger. However, rather than taking the time and expense to bury the cables linking the stands to the electronics shelter, the cables were run through aboveground conduit. (Only 16 stands were actually cabled to the shelter.) A copy of the LWA1 TBN digital system was installed in the shelter, along with LWA1-style digital storage units. For most of these elements, spare parts from the LWA1 construction were used, to minimize the impact on DTRA. Unfortunately, it turned out that the TBN unit was faulty; troubleshooting and repair imposed additional delay in completing the outrigger. The system was completed in February 2012. An image of the outrigger site is shown in figure 11.

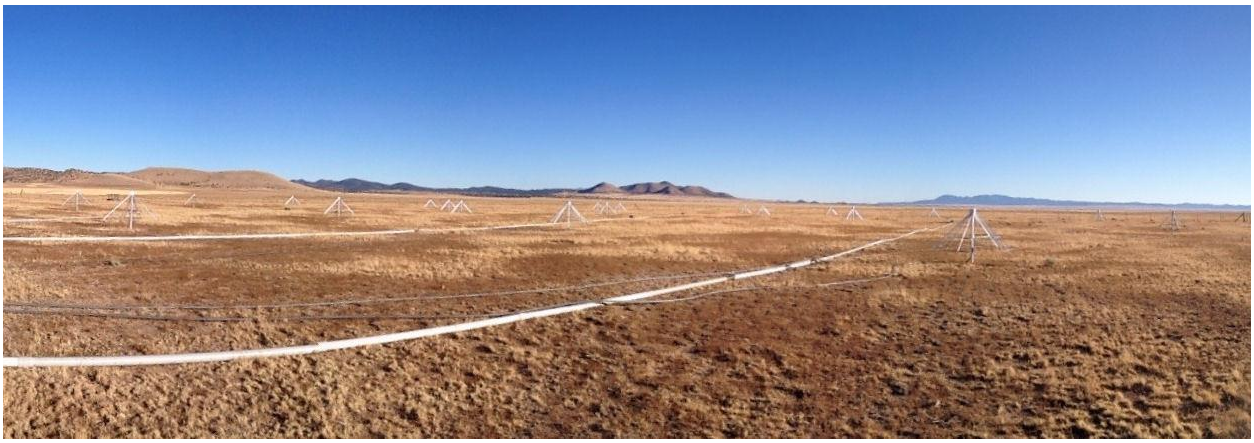

Figure 11: Antenna stands distributed over the outrigger site.

Unfortunately, initial TBN imagery (March 2012) from the outrigger has been plagued with RFI, similar to the problem seen originally at LWA1. A time series from a single antenna (figure 12) shows the impulsive, random nature of the emission. A survey of the potential local sources, however, suggests that most of the power lines in the vicinity are producing emission. The tentative conclusion is that these rural power lines are infrequently maintained, so that the components are allowed to degrade so long as they do not interrupt power delivery. Resolution of the problem will require extensive work with Socorro Electric Cooperative. For now, the plan to incorporate outrigger data to reduce confusion noise must be tabled.

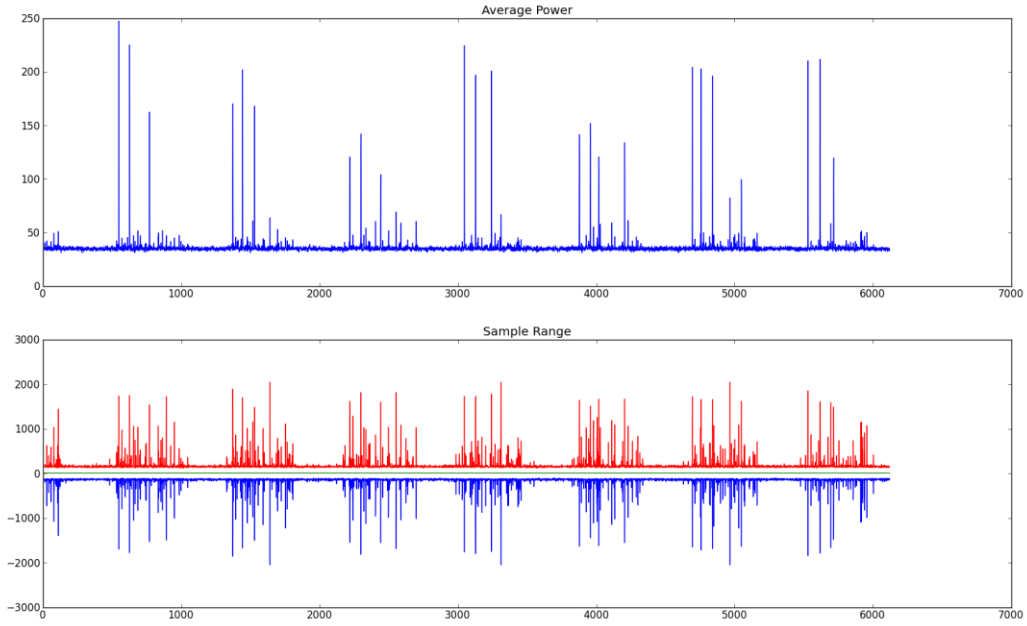

Figure 12: Sample outrigger antenna power time series, showing impulsive RFI.

III. ANALYSIS PROCEDURE

The initial plan for riometric analysis was based on the calibration scheme for the full LWA, known as 'flickering'. With 256 antennas, the sensitivity of an LWA station is sufficient to reach a thermal rms of 0.93 Jy/beam in 20 milliseconds. This would be sufficient to provide 10-sigma detections of the brightest 362 sources in the 74 MHz VLA Low-Frequency Sky Survey (VLSS) catalog[12], shown in figure 13a. Of course, as illustrated in figure 13b, only a subset of those sources will be visible to LWA1 at a given time. However, analysis by Cohen and Paravastu[13] of the details of the source distribution indicate that, over the course of a day, there are at least 100 sources observable. They calculate that, allowing for a cycle time of 50 milliseconds, it would be possible to observe all the accessible sources in the list of 362 within roughly 6 seconds. Because the ionosphere is relatively stable over that timescale, they suggested that 'flickering' a dedicated beam over these sources would suffice to provide a reasonable characterization of the ionosphere above the array.

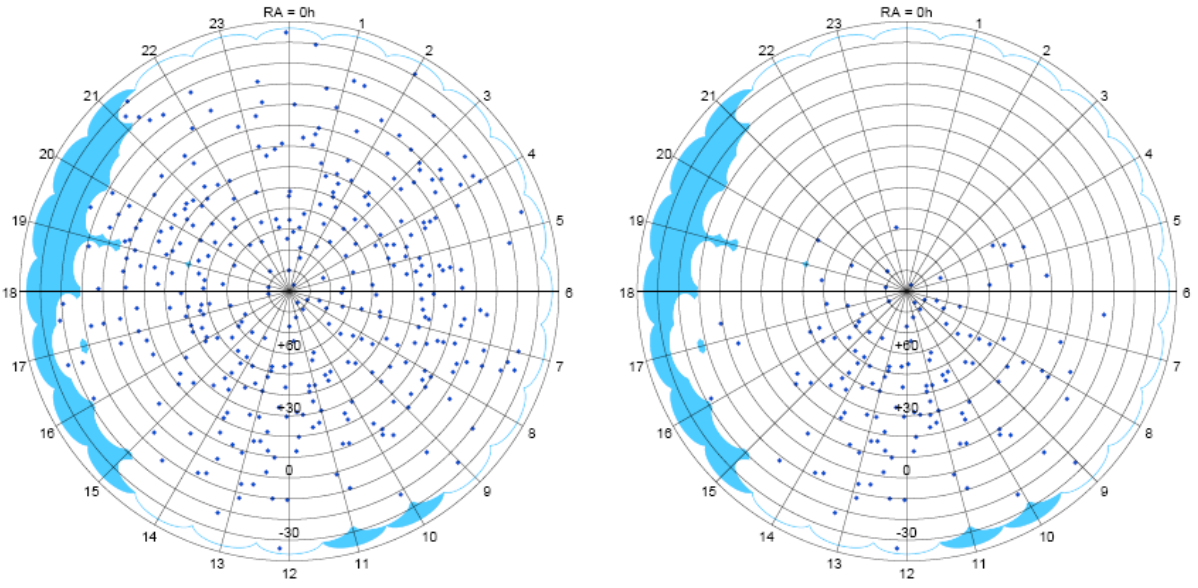

Figure 13: (a) The 362 sources in the VLSS database that can be detected at the 10-sigma level by the LWA within 20 milliseconds; (b) the subset of those sources visible at a particular moment above the array.

The riometric plan, then, was to measure the accessible sources and fit a simple model ionosphere using a 'tipping curve' (described below). The problem, however, is that with the large beam size of the single LWA1 station, the confusion noise dominates at a level of roughly 25 Jy/beam. Integrating longer than 1 millisecond with LWA1 is purposeless. This was the rationale for building the outrigger station.

The alternative is to work with the TBN data, fitting the ionosphere over the bright part of the background seen in the all-sky image. The tipping curve procedure assumes that the ionosphere above the station can be approximated as a horizontal slab. In that case, the opacity

of the ionosphere varies away from the zenith primarily because of the longer pathlength through the slab, proportional to the cosecant of the zenith angle. If the sky provides a uniform background over the region being fit, then one can plot the variation with csc(z.a.) and extrapolate the fitted line to zero. This 'zero air mass' value gives us the background brightness, and one can substitute it back in to get the zenith attenuation. (This is a standard method for calibrating microwave radiometers, where the corresponding parameters are the atmospheric brightness and the water-vapor absorption.)

While the raw TBN images would have sufficed as the starting point for these fits, the fact that the PASI data stream would be available independently and on a real-time basis made it more desirable. This required the initial development of additional software for PASI, to prepare an output data stream in raw floating-point format together with metadata (as opposed to the original image format); and to locate, fit, and remove point sources from the data.

The final analysis procedure to be implemented is more complex. A top-level summary is shown in the Appendix.

IV. CALIBRATION PROBLEMS

In order to do the analysis, it is necessary that the raw image data be reasonably stable – for example, significant gain variations over the PASI data cycle will be disruptive. There is no evidence for any significant gain instability in the LWA1 system. In close analysis of the data, however, an unexpected problem was found. This has been dubbed 'shimmering'.

Figure 14 shows the fluxes for the two bright point sources, Cyg A and Cas A, as derived from the PASI data fits over the course of a single day. The flux scale ('Jansky-ish') is set by presuming that Cyg A will be 16,000 Jy at culmination. The overall variation is with zenith angle, and represents the combination of antenna beam response, station beam variation with zenith angle, and ionospheric absorption. However, the scatter in the curves is far too large to be thermal, or even confusion, noise. It is also much larger than any extreme problem with the system gains.

A more extreme example can be seen in excerpts from the 25 MHz PASI data for MJD 55928 (2 January 2012), shown in figure 15. Over the course of a mere 55 seconds, the flux of Vir A drops dramatically. The phenomenon is particularly striking in the movie made from these data, available at http://www.phys.unm.edu/~lwa/lwatv/55928.mov.

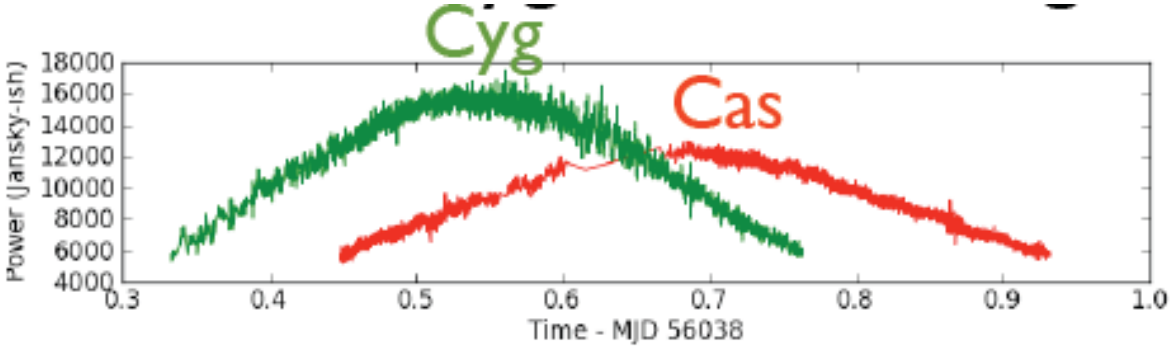

Figure 14: Fitted flux 'shimmering' observed in PASI measurements for Cyg A and Cas A.

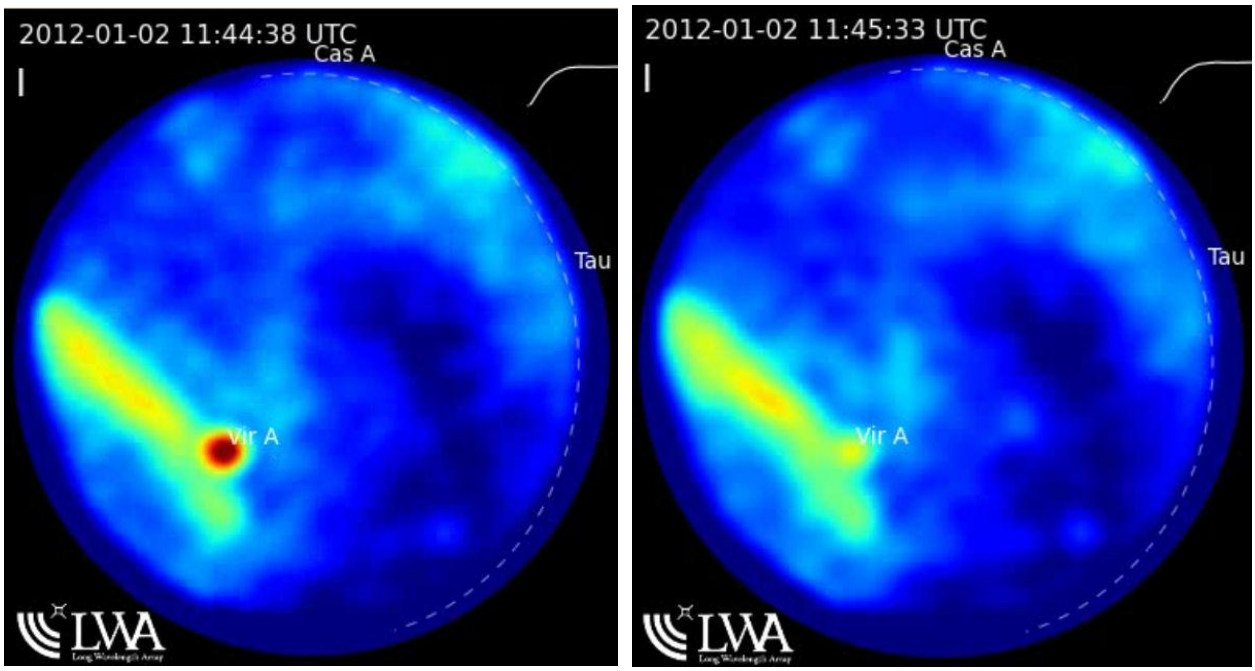

Figure 15: PASI 25 MHz images on 2 January 2012, separated by 55 seconds. Note the dramatic change in the apparent flux of Vir A.

Although the phenomenon is most apparent in the variations of bright sources, it is not limited to them. This is unfortunate, as it eliminates some of the more straightforward solutions, such as pointing changes. Figure 16 shows the mean and RMS power for 1,000 fixed positions on the sky, chosen randomly except for restricting them to locations without either point sources or significant Galactic emission. Tracked over the course of a day, they show similar shimmering effects. In addition, there is a minimum value for the RMS of roughly 50 Jy. (Again, the scale is only calibrated by taking a flux of 16,000 Jy for Cyg A at culmination.) This makes it difficult to explain the phenomenon by scintillation, which would have a distribution down to zero.

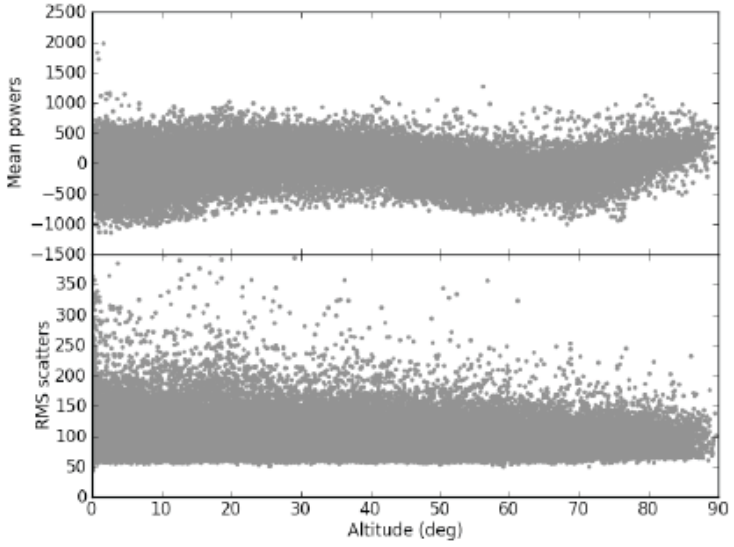

Figure 16: Mean and RMS power in 1,000 random 'blank' positions.

One hypothesis for this phenomenon is currently under investigation. When strong signals from RFI or solar bursts illuminate the station beam, it becomes clear that the sidelobe pattern of the station beam is far more complex – 'mottled' – than predicted by simulations. An example is shown in figure 17. Here, a solar burst is bringing out the nearer Airy ring; rather than being relatively smooth, it is quite structured. With such complex sidelobes, it can be argued that power from the structured background far from the center of the station beam could make a rapidly fluctuating contribution to the flux scale, and thus a shimmering effect.

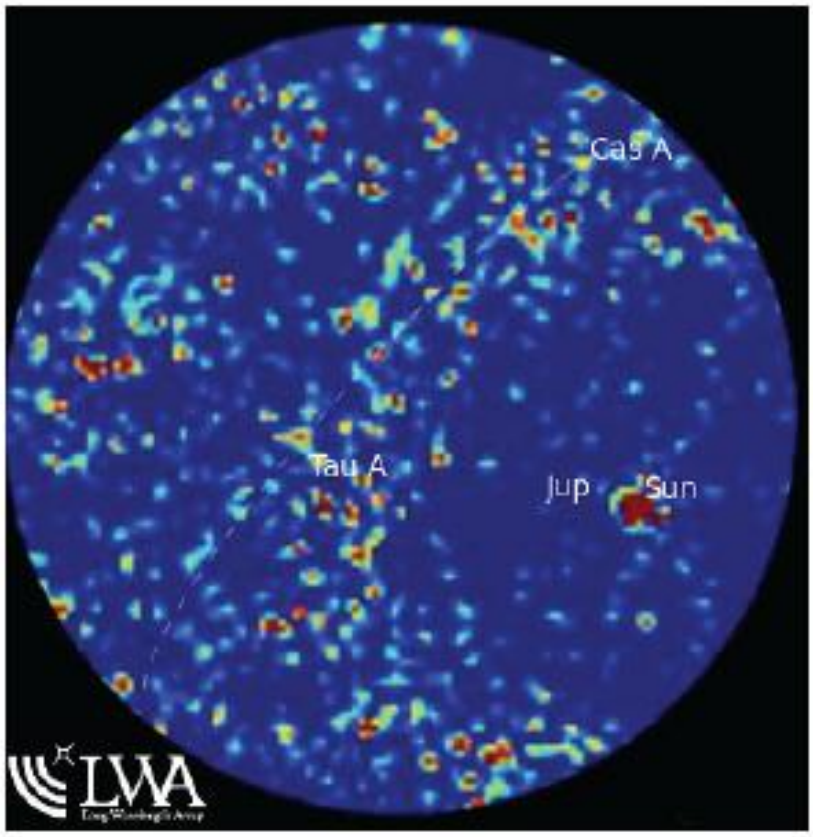

Figure 17: Highly structured sidelobe illuminated by solar burst.

V. SUMMARY

Despite the straightforward nature of the LWA1 instrument, the complexities of low-frequency array phenomenology and the difficulties of working in a surprisingly RFI-rich environment have prevented collection and analysis of all-sky data to show anomalous ionospheric absorption events. Given the pace at which problems have been resolved during the project, it is reasonable to expect that useful data collection will be possible within the calendar year. Nonetheless, a significant hardware augmentation of the LWA1 station has been completed, and the analysis process for riometric measurements has been established.

As the PASI data stream is a continuous output for LWA1, it will be feasible to insert the riometric analysis into the standard data products, requiring essentially no further investment in

hardware or software development. It is intended to follow up on this work in that mode. With patience, the desired absorption events should turn up.

This work was done with the support of Joseph Craig, LWA system engineer, Jayce Dowell, LWA system programmer and LWA postdoc, Jake Hartman, PASI developer and LWA postdoc, and Gregory Taylor, LWA Principal Investigator, together with the labor of a number of students who assisted at the outrigger site.

VI. REFERENCES

1) *e.g.*, Vainio *et al*. 2009, *Space Science Reviews*, **147**#3/4, 187-231.
2) Bucik *et al*. 2006, *Ann Geophys*, **24**#7, 1969-1976.
3) Pulinets 2004, *TAO*, **15**#3, 413-435.
4) *e.g.*, Orsolini *et al*. 2005, *Geophys. Res. Lett.*, **32**, L12S01, doi:10.1029/2004GL021588.
5) *e.g.*, Demirkol *et al*. 1999, *Geophys. Res. Lett.*, **26**#23, 3557-3560.
6) Mitra and Shain 1953, *J. Atm. Terr. Physics*, **4**#4/5, 204-218.
7) Little and Leinbach 1959, *Proc. IRE*, **47**#2, 315-320.
8) Bortnik et al, *J. Geophys. Res.*, **111**, A12216, doi:10.1029/2006JA011802.
9) http://aurora.phys.ucalgary.ca/norstar/rio/info.html
10) S.W. Ellingson et al., "The Long Wavelength Array," 2009, Proc. IEEE, **97#**8, 1421–30.
11) G.B. Taylor et al. , "First Light for the First Station of the Long Wavelength Array," submitted. Preprint available as Long Wavelength Array Memo 185 at http://www.ece.vt.edu/swe/lwa/.
12) Cohen, A. S., Lane, W. M., Cotton, W. D., Kassim, N. E., Lazio, T. J. W., Perley, R. A., Condon, J. J., & Erickson, W. C. 2007b, AJ, **134**, 1245
13) Cohen, A. S., and Paravastu, N. , Long Wavelength Array Memo 128, at http://www.ece.vt.edu/swe/lwa/.

VII. APPENDIX – DATA ANALYSIS SOFTWARE SCHEMATIC

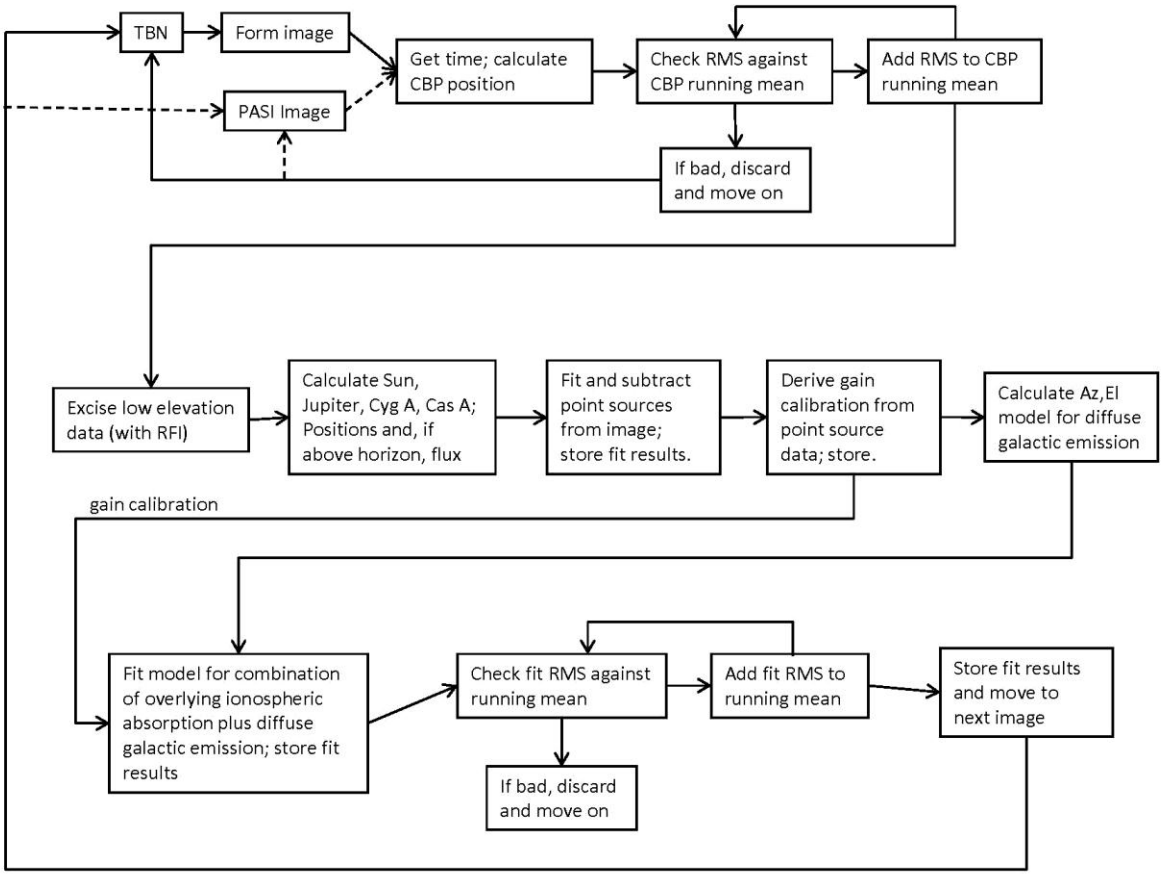

Figure 18: Analysis schematic for riometric measurements with LWA1.

DEPARTMENT OF DEFENSE

DEFENSE THREAT REDUCTION
AGENCY
8725 JOHN J. KINGMAN ROAD
STOP 6201
FORT BELVOIR ,VA 22060
ATTN: J. REED

DEFENSE THREAT REDUCTION
AGENCY
8725 JOHN J. KINGMAN ROAD
STOP 6201
FORT BELVOIR ,VA 22060
ATTN: R. KEHLET

DEFENSE TECHNICAL
INFORMATION CENTER
8725 JOHN J. KINGMAN ROAD,
SUITE 0944
FT. BELVOIR, VA 22060-6201
ATTN: DTIC/OCA

DEPARTMENT OF DEFENSE CONTRACTORS

EXELIS, INC.
1680 TEXAS STREET, SE
KIRTLAND AFB, NM 87117-5669
ATTN: DTRIAC

OFFICE OF THE VICE PRESEIDENT
FOR RESEARCH
UNIVERSITY STRATEGIC
PARTNERSHIP
1 UNIVERSITY OF NEW MEXICO
ALBUQUERQUE, NM 87131